crosslinker (*N*-succinimidyl 3-[2-pyridyldithio]-propionate; Thermo Fisher) for 30 minutes on ice. SPDP-modified IgGs and thiolated NCS were separately purified using NICK columns (GE Healthcare). They were then mixed for 8 hours at room temperature. IgG-NCS were purified with a Superdex 200 column. Modification efficiency was quantified after sodium-dodecyl sulfate-polyacrylamide gel electrophoresis using a Gel DOC EZ system and Image laboratory software (Bio-Rad Laboratories, Inc., Hercules, CA).

Labeling of purified mAbs

For fluorescent labeling, mAbs were labeled using Cy5.5-NHS (GE Healthcare). For ^{125}I labeling, 100 μg mAbs in 0.4 M phosphate buffer were labeled with 0.2 mCi Na^{125}I (PerkinElmer, Inc., Waltham, MA) based on the chloramine-T method.[38] For biotin labeling, mAbs were biotinylated using EZ-Link Sulfo-NHS-Biotin (Thermo Fisher). Each mAb was purified using a NICK desalting column (GE Healthcare).

Flow cytometry

Cy5.5-labeled mAb (mAb$^{Cy5.5}$; 4 μM) was incubated with 5.0×10^5 cells of MS1 cells in 6-well plates for 2 hours at 4°C. After washing three times, the cells were incubated for an additional 0.5 to 8 hours at 37°C. At each time point, cells were collected in 2-mM ethylenediaminetetraacedtic acid/PBS. Bound mAbs were digested using 0.1% trypsin/PBS at 37°C for 20 minutes (trypsinized group) or PBS (nontrypsinized group). Cellular fluorescence was measured by Gallios flow cytometer (Beckman Coulter, Inc., Miami, FL). The ratio of internalization was calculated using the following formula: internalization (%) = {internalized mAb$^{Cy5.5}$}/{total bound mAb$^{Cy5.5}$} × 100 (%) = {(MFI of mAb)$_T$ − (MFI of anti-His [mAb])$_T$}/{(MFI of mAb)$_N$ − (MFI of anti-His[mAb])$_N$} × 100 (%). MFI indicates mean fluorescence intensity. T and N indicate trypsinized and nontrypsinized groups, respectively.

In vivo biodistribution

dscFvs^{125I} (0.2 nmol) was intravenously injected into B16BL6 tumor–bearing mice. At 2 hours and 24 hours after injection, the radioactivity of each organ was counted using the Wizard 2480 γ-ray counter (PerkinElmer). %ID/g tissue was calculated using following formula: %ID/g tissue = (count/g tissue)/(total injected count) × 100 (%). Two individual experiments were combined for the final data (total 11 mice/group).

Immunofluorescence of the tissue sections

B16BL6 tumor–bearing mice were administered 2 nmol of dscFvs^{Bio}. At 2 hours after the injection, the tumors, kidneys, and hearts were embedded in optimal cutting temperature compound (Sakura Finetek, Inc., Torrance, CA) and frozen in liquid nitrogen. Thin sections (7 μm) were prepared using a Cryostat CM1850 (Leica Microsystems GmbH, Wetzlar, Germany) and fixed in 4% paraformaldehyde. DscFvs^{Bio} in the sections were stained with streptavidin phycoerythrin conjugate (eBioscience Inc., San Diego, CA) in Dako REAL Antibody Diluent (DAKO Corporation, Carpinteria, CA). CD31+ vascular endothelial cells were stained with rat anti-CD31 antibody (MEC13.3; Becton Dickinson and Company, Franklin Lakes, NJ) in Dako REAL Antibody Diluent and Alexa488 conjugated anti-rat IgG (A11006; Invitrogen). The samples were embedded with Prolong Gold antifade reagent with 4′,6-diamidino-2-phenylindole (Invitrogen) and observed with a fluorescence microscope FSX100 (Olympus Corporation, Tokyo, Japan).

In vivo therapy experiments

Activities of scFv-PSIFs and IgG-NCSes were confirmed by WST-8 assay as described before. B16BL6 cells were inoculated intracutaneously into C57BL6 mice (Japan SLC) on day 0. Mice were intravenously injected with 15 pmol scFv-PSIFs and 10 pmol IgG-NCSs on days 3, 5, 7, 9, and 11 (7 mice/group). The volume of the tumor was calculated according to the following formula: tumor volume (mm^3) = {major axis of tumor (mm)} × {minor axis of tumor (mm)}^{2} × 0.4.

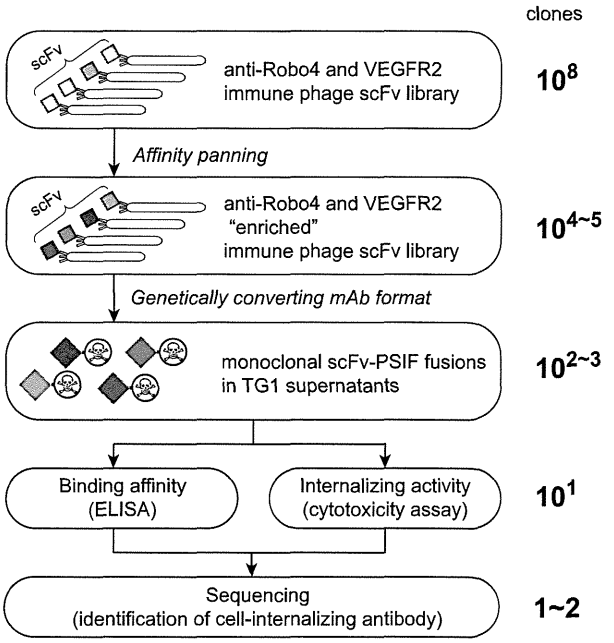

Figure 1. Phage display-based method to search for cell-internalizing mAbs. The phage antibody library was "enriched" by affinity panning against the desired antigens. Plasmids encoding scFvs were collected from TG1 *E coli* strains infected by "enriched" phage libraries. Genes of scFvs were digested out and ligated into a PSIF fusion protein expression vector. These plasmids were then transformed to TG1, and then single colonies were picked up. From these individual colonies, monoclonal scFv-PSIF fusions were induced in TG1 supernatants. Using these fusion proteins, binding affinities and internalizing activities of several hundreds of scFv-PSIFs were easily estimated by ELISA and cytotoxicity assays, respectively. Finally, genes of positive scFvs were collected from TG1, and cell-internalizing scFvs were identified by sequencing. In this report, we used anti-Robo4 and anti-VEGFR2 immune phage scFv libraries as the phage antibody libraries, and mRobo4 and mVEGFR2 as the desired antigens.

Results

High-throughput screening for cell-internalizing mAbs

To identify cell-internalizing mAbs, we applied the phage immune scFv library to high-throughput screening of cell-internalizing molecules based on the PSIF system[8] (Figure 1). Our anti-Robo4 or anti-VEGFR2 phage library comprised approximately 3.0×10^8 or 5.0×10^8 independent scFvs, which was validated by sequence analysis. To assess the qualities of the libraries, affinity panning was performed against each antigen. During the panning, output phages were increased, suggesting that the desired scFvs were enriched in the library (supplemental Figure 1A-B,E-F). After the fourth panning, >40% of monoclonal scFvs showed specific binding in enzyme-linked immunosorbent assay (ELISA) (supplemental Figure 1C-D,G-H).

To validate the efficacy of cell-internalizing mAbs in a mouse model, we selected libraries enriched against murine antigens (mRobo4 and mVEGFR2) and chose MS1 murine endothelial cells for the screening of cell-internalizing mAbs because we confirmed the expressions of both mRobo4 and mVEGFR2 in MS1 cells using reverse transcriptase–polymerase chain reactioin. For the screening, scFv genes obtained after the fourth round of panning were cloned into the PSIF expression vector. Monoclonal scFv-PSIFs were expressed in TG1 supernatants (315 clones per library). For anti-Robo4s, 178 of 315 clones bound to mRobo4 in ELISA and 20 of these 178 binders were cytotoxic against MS1 cells

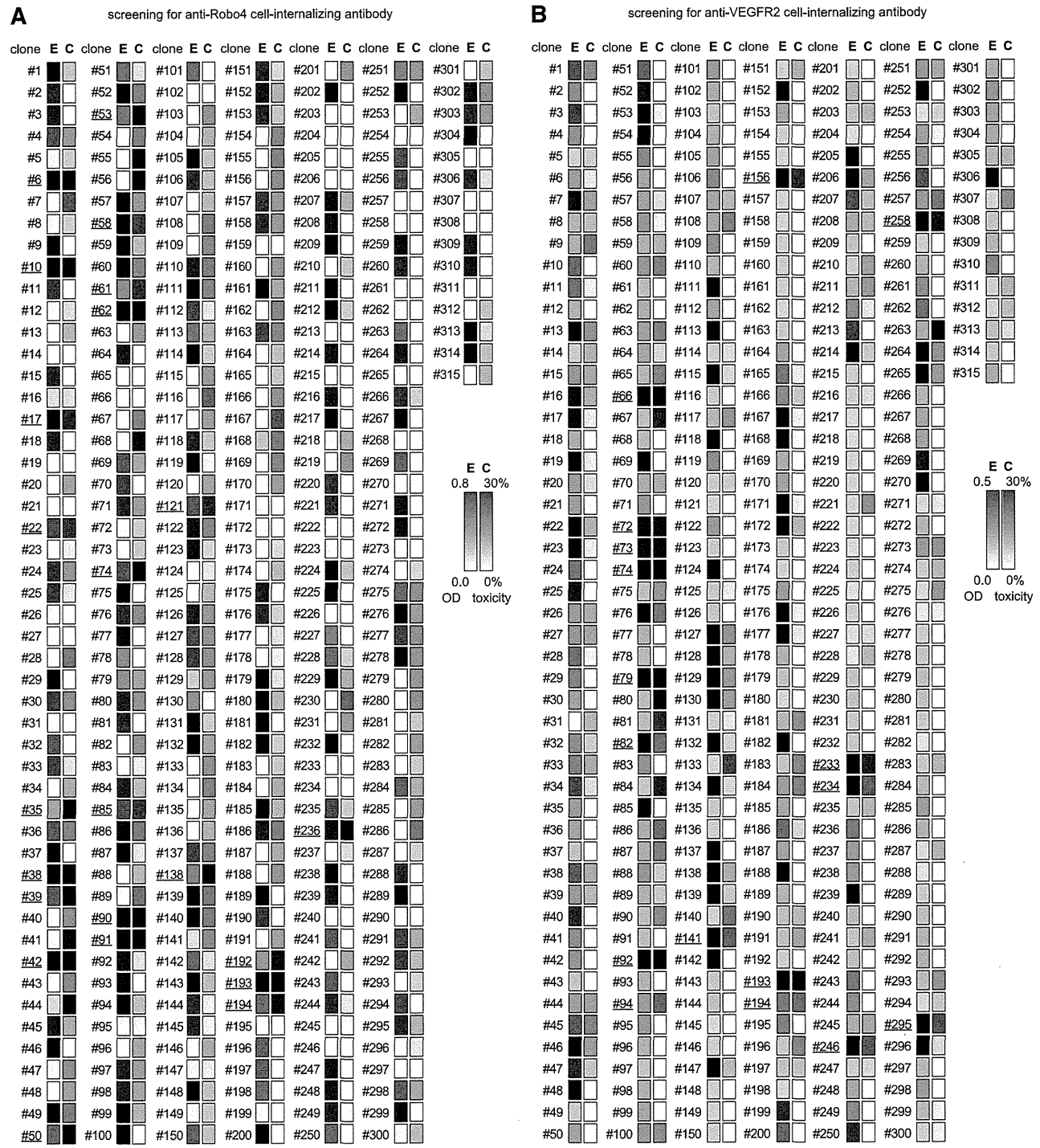

Figure 2. Screening of cell-internalizing mAbs (ELISA and cytotoxicity assay). To screen for cell-internalizing mAbs, 315 clones per antigen were analyzed by ELISA and cytotoxicity assay. (A) Result for Robo4, (B) Result for VEGFR2. Monoclonal scfv-PSIFs were induced in TG1 supernatant. The binding properties and cytotoxicities to MS1 cells were then assessed by an ELISA and WST-8 assay, respectively. E, ELISA results; C, WST-8 assay results. Individual results from ELISA (OD = 0.8 or 0.5~0.0) and WST-8 assay (cytotoxicity = 30%~0%) were mapped in grayscale densities. The 24 candidates against Robo4 and 17 candidates against VEGFR2 are indicated by the underline (ELISA OD ≥0.2 and cytotoxicity ≥20%). After omitting redundant clones by sequencing, 1 cell-internalizing mAb and 2 low-internalizing mAbs against mRobo4, and 2 cell-internalizing mAbs and 14 low-internalizing mAbs against mVEGFR2 were identified.

(Figure 2A). In a similar manner, for anti-VEGFR2s, 156 of 315 clones bound to VEGFR2 and 17 of the 156 binders were positive in the ELISA and cytotoxicity assays (Figure 2B). Sequence analysis to omit redundant clones revealed that these clones comprised 1 anti-Robo4 cell-internalizing mAb, 2 anti-Robo4 low-internalizing mAbs, 2 anti-VEGFR2 cell-internalizing mAbs, and 14 anti-VEGFR2 low-internalizing mAbs. For anti-Robo4s, only one anti-Robo4 cell-internalizing mAb was named "R4-13i" and a low-internalizing mAb with high affinity and low cytotoxicity was named "R4-16." In a similar manner, "V2-05i" and "V2-02" were selected as an anti-VEGFR2 cell-internalizing mAb and a low-internalizing mAb, respectively. After purification of the recombinant proteins, both anti-Robo4 scFvs bound to hRobo4, similar to mRobo4. Conversely, anti-VEGFR2 scFvs bound to

Table 1. Binding kinetics of antibodies in surface plasmon resonance analysis

Antibody	Target	Format	k_a ($M^{-1}s^{-1}$)	k_d (s^{-1})	K_D (M)
R4-13i	mRobo4	scFv	$1.25 \pm 0.36 \times 10^5$	$5.82 \pm 0.95 \times 10^{-4}$	$5.03 \pm 1.95 \times 10^{-9}$
(internalizing)		dscFv	$1.15 \pm 0.34 \times 10^6$	$5.98 \pm 0.61 \times 10^{-4}$	$5.64 \pm 2.21 \times 10^{-10}$
		IgG	$1.14 \pm 0.55 \times 10^6$	$4.19 \pm 1.70 \times 10^{-4}$	$2.22 \pm 0.51 \times 10^{-10}$
		scFv-PSIF	$7.22 \pm 4.31 \times 10^4$	$4.28 \pm 1.60 \times 10^{-3}$	$6.47 \pm 1.61 \times 10^{-8}$
		IgG-NCS	$1.02 \pm 0.15 \times 10^6$	$4.66 \pm 0.86 \times 10^{-4}$	$4.59 \pm 0.74 \times 10^{-10}$
R4-16	mRobo4	scFv	$1.30 \pm 0.33 \times 10^5$	$5.82 \pm 1.50 \times 10^{-4}$	$4.77 \pm 1.96 \times 10^{-9}$
(low-internalizing)		dscFv	$1.12 \pm 0.03 \times 10^6$	$5.91 \pm 1.50 \times 10^{-4}$	$5.31 \pm 1.96 \times 10^{-10}$
		IgG	$1.06 \pm 0.24 \times 10^6$	$3.60 \pm 0.85 \times 10^{-4}$	$2.76 \pm 0.16 \times 10^{-10}$
		scFv-PSIF	$8.90 \pm 1.42 \times 10^4$	$6.10 \pm 2.45 \times 10^{-3}$	$7.24 \pm 3.74 \times 10^{-8}$
		IgG-NCS	$1.07 \pm 0.12 \times 10^6$	$3.93 \pm 0.54 \times 10^{-4}$	$3.72 \pm 0.89 \times 10^{-10}$
V2-05i	mVEGFR2	scFv	$9.66 \pm 3.57 \times 10^4$	$4.40 \pm 0.95 \times 10^{-4}$	$5.13 \pm 2.61 \times 10^{-9}$
(internalizing)		dscFv	$8.75 \pm 2.03 \times 10^5$	$5.59 \pm 2.57 \times 10^{-4}$	$6.16 \pm 1.47 \times 10^{-10}$
		IgG	$1.14 \pm 0.09 \times 10^6$	$3.21 \pm 0.35 \times 10^{-4}$	$2.84 \pm 0.52 \times 10^{-10}$
		scFv-PSIF	$9.57 \pm 0.84 \times 10^4$	$6.51 \pm 1.87 \times 10^{-3}$	$6.94 \pm 2.63 \times 10^{-8}$
		IgG-NCS	$0.96 \pm 0.06 \times 10^6$	$4.37 \pm 0.90 \times 10^{-4}$	$4.52 \pm 0.79 \times 10^{-10}$
V2-02	mVEGFR2	scFv	$7.94 \pm 1.24 \times 10^4$	$4.28 \pm 3.23 \times 10^{-4}$	$5.07 \pm 3.05 \times 10^{-9}$
(low-internalizing)		dscFv	$8.94 \pm 2.55 \times 10^5$	$5.57 \pm 1.25 \times 10^{-4}$	$6.60 \pm 2.39 \times 10^{-10}$
		IgG	$1.13 \pm 0.22 \times 10^6$	$3.25 \pm 1.10 \times 10^{-4}$	$2.90 \pm 0.98 \times 10^{-10}$
		scFv-PSIF	$9.84 \pm 1.52 \times 10^4$	$5.75 \pm 2.05 \times 10^{-3}$	$5.81 \pm 1.93 \times 10^{-8}$
		IgG-NCS	$1.08 \pm 0.08 \times 10^6$	$5.25 \pm 1.58 \times 10^{-4}$	$4.85 \pm 1.30 \times 10^{-10}$

Binding kinetics were analyzed against mRobo4 (R4-13i and R4-16) or mVEGFR2 (V2-05i and V2-02). Values are shown as means ± SD from three different preparations.

k_a, association rate constant ($M^{-1}s^{-1}$); k_d, dissociation rate constant (s^{-1}); K_D, equilibrium dissociation constant (k_d/k_a) (M).

mVEGFR2, but not to hVEGFR2. We also confirmed using competitive ELISA that the mAbs did not share their antigen-binding epitopes (supplemental Figure 2).

Characterization of mAbs

We purified scFvs, dimerized scFvs (dscFvs), IgGs, and scFv-PSIF as recombinant proteins. IgGs conjugated with neocarzinostatin (IgG-NCSes) were also prepared for in vivo experiments. NCSes were confirmed to be conjugated to IgG molecules in the purified IgG-NCS fraction, and the efficiencies of the NCS modifications were similar in all IgG-NCSes (1.6~1.8 NCSes per single IgG). Surface plasmon resonance analysis revealed that cell-internalizing mAbs and low-internalizing mAbs had similar affinities against antigens in all antibody forms (Table 1).

To quantify the internalization, flow cytometry analysis was performed with Cy5.5-labeled mAbs ($scFv^{Cy5.5}$, $dscFv^{Cy5.5}$, and $IgG^{Cy5.5}$; Figure 3A,C). After $mAbs^{Cy5.5}$ bound to the cell surface, internalization was induced by incubation at 37°C for 2 hours. By removing cell-surface $mAbs^{Cy5.5}$ with trypsinization, the internalized $mAbs^{Cy5.5}$ were quantified by flow cytometry. At 2 hours, approximately 30% of cell-internalizing mAbs remained after trypsinization, whereas most of the low-internalizing mAbs were degraded (Figure 3A,C). This result clearly suggested that the internalization efficiencies differed between cell-internalizing mAbs and low-internalizing mAbs, even among the three different mAb forms. In a similar manner, a time-shift analysis revealed that >40% of cell-internalizing mAbs were internalized after 8 hours of incubation (Figure 3B,D). These findings indicate that only cell-internalizing mAbs were efficiently internalized into the cells, although low-internalizing mAbs had affinities similar to those of cell-internalizing mAbs (Table 1).

Intracellular localization

The intracellular behaviors of cell-internalizing mAbs were analyzed with a confocal laser-scanning microscope. In MS1 cells, intracellular fluorescence derived from $scFv^{Cy5.5}$ was observed with cell-internalizing scFvs, but not with low-internalizing scFvs (supplemental Figure 3A,D,E,H). Fluorescence was suppressed, however, under the inhibition of energy-dependent endocytosis (supplemental Figure 3B-C,F-G). These results suggested that cell-internalizing scFvs entered into the cells via energy-dependent endocytosis.

For in-depth analysis of the intracellular behavior, confocal laser-scanning microscope analysis was performed with immunostaining of endosome markers (supplemental Figure 3Iab). After $scFvs^{Cy5.5}$ were bound to the cell-surface, the cells were incubated for an additional 1 to 8 hours at 37°C. The early endosome marker, early endosome antigen 1 (EEA1), and the late endosome marker, lysosomal-associated membrane protein 1 (LAMP1), were visualized using Alexa488-conjugated antibodies. Colocalization with EEA1+ early endosomes decreased over time (supplemental Figure 3I-M,S-W), whereas colocalization with LAMP1+ late endosomes increased (supplemental Figure 3N-R,Xab). These findings suggested that cell-internalizing scFvs were encapsulated in EEA1+ early endosomes at an early stage and eventually accumulated in LAMP1+ late endosomes. This is thought to be a typical endocytotic molecular sorting pathway.[39]

Influence of cell-internalizing activity on biodistribution

To assess the biodistribution of cell-internalizing mAbs, ^{125}I-labeled dscFvs ($dscFv^{125I}$) were intravenously injected into B16BL6 tumor-bearing mice. In this experiment, we selected the dscFv form because dscFv has superior in vivo tumor-targeting potency compared with scFv.[40] At 2 hours, the tumor distribution of anti-Robo4 and anti-VEGFR2 $dscFvs^{125I}$ was similar to but significantly higher than that of a negative control $dscFv^{125I}$ (anti-His[dscFv]^{125I}; Figure 4A-B). This finding suggested that the anti-Robo4 and anti-VEGFR2 dscFvs had tumor-targeting properties. Anti-Robo4 $dscFvs^{125I}$ also accumulated in the kidney, indicating a nonspecific distribution of dscFvs for their elimination,[41,42] because no significant difference was observed between anti-Robo4 $dscFvs^{125I}$

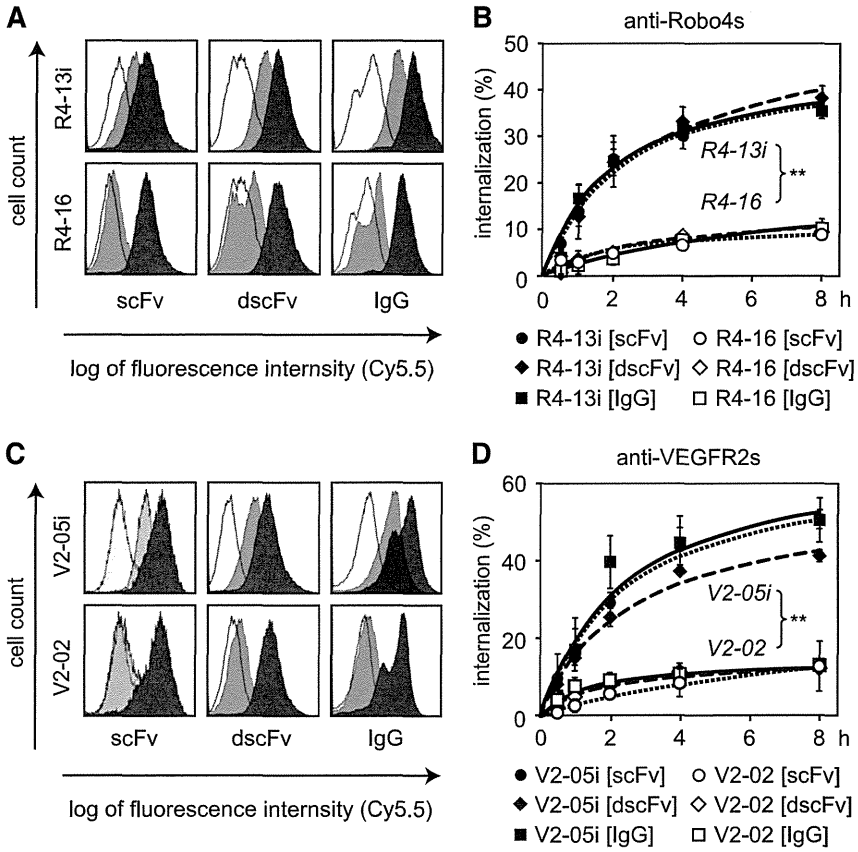

Figure 3. Cell internalization analyzed by flow cytometry. (A,C) Trypsinization to quantify internalized mAbs. Different forms of $mAbs^{Cy5.5}$ bound to the MS1 cells at 4°C. After washing out the unbound mAbs, internalization was induced for 2 hours at 37°C. To detect only internalized mAbs, cell surface proteins were trypsinized. The remaining cellular fluorescence was then analyzed by flow cytometry. (A) Anti-Robo4 $mAbs^{Cy5.5}$, (C) Anti-VEGFR2 $mAbs^{Cy5.5}$. Black, nontrypsinized group; gray, trypsinized group; white, negative control (anti-His[scFv]$^{Cy5.5}$, anti-His[dscFv]$^{Cy5.5}$, or anti-FLAG [IgG]$^{Cy5.5}$). (B,D) Time course of the internalization. After binding at 4°C, internalization was induced for 0.5, 1, 2, 4, or 8 hours at 37°C. The ratio of internalization was calculated using the following formula: internalization (%) = {internalized mAb}/{total bound mAb} × 100 (%) = {(MFI of mAb)$_T$ − (MFI of negative control)$_T$}/{(MFI of mAb)$_N$ − (MFI of negative control)$_N$} × 100 (%). T, trypsinized group; N, nontrypsinized group; MFI, mean fluorescence intensity. (B) Closed and open markers indicate R4-13i and R4-16, respectively. (D) Closed and open markers indicate V2-05i and V2-02, respectively. (B,D) Circles, diamonds, and squares indicate scFv, dscFv, and IgG, respectively. Each experiment was performed in triplicate. Values are shown as means ± SD. $^{**}P < .01$; internalizing mAb versus low-internalizing mAb in each form by 2-way ANOVA (n = 3).

and anti-His[dscFv]^{125I} (Figure 4A). Importantly, the accumulation of anti-VEGFR2 $dscFvs^{125I}$ in the kidney was significantly greater than that of anti-His[dscFv]^{125I} (Figure 4B). A similar accumulation of anti-VEGFR2 $dscFvs^{125I}$, but not anti-Robo4 $dscFvs^{125I}$ (Figure 4A), was observed in the heart (Figure 4B).

To confirm this phenomenon, the localization of dscFvs in the tissues was analyzed by immunofluorescence studies (Figure 4E-S). Biotin-labeled dscFvs ($dscFvs^{Bio}$) were intravenously administered to B16BL6 tumor–bearing mice and the tumors, kidneys, and hearts were extracted 2 hours after injection. The $dscFv^{Bio}$ and vascular endothelial cells were stained by streptavidin-AP and anti-CD31 antibody, respectively. In the tumor sections, all of the anti-Robo4 and anti-VEGFR2 $dscFvs^{Bio}$ were clearly detected with CD31+ tumor blood vasculature, whereas anti-His[dscFv]^{Bio} was not detectable (Figure 4E,H,K,N,Q). This finding suggested that both anti-Robo4 and anti-VEGFR2 dscFvs recognized tumor endothelial cells in vivo, which contributed to their accumulation in the tumor. Interestingly, in the kidney and heart sections, signals around CD31+ blood vasculature were detectable only with the anti-VEGFR2 $dscFvs^{Bio}$, and not with anti-Robo4 $dscFvs^{Bio}$ or anti-His[dscFv]^{Bio} (Figure 4F-G,I-J,L-M,O-P,R-S). This finding was compatible with the biodistribution results (Figure 4A-B), which suggested that anti-VEGFR2 dscFvs recognized VEGFR2 on normal blood vessels because VEGFR2 plays an important role in normal tissues, including the kidney and heart.[31-33] No specific accumulation of anti-Robo4 dscFvs was observed in normal tissues, suggesting that the anti-Robo4 mAbs were useful for specific tumor vascular targeting.

Comparison of the cell-internalizing mAbs and low-internalizing mAbs revealed a significantly greater accumulation of cell-internalizing $dscFvs^{125I}$ in the tumors compared with low-internalizing $dscFvs^{125I}$ at 24 hours (Figure 4C-D), whereas no differences were observed at 2 hours (Figure 4A-B). This finding suggested that cell-internalizing mAbs were retained in the tumor for a longer time than the low-internalizing mAbs. This phenomenon was also observed in the kidney and heart with the anti-VEGFR2 dscFvs (Figure 4D). This retention might be caused by the mAb internalization, which allowed the mAb to escape from the bloodstream and accumulate in the tumor blood endothelial cells. Taken together, these results suggest that mAb internalization into the tumor endothelium improves mAb-based drug-delivery in vivo.

Enhanced antitumor effect depends on the cell-internalizing activity

To assess the antitumor potencies of the cell-internalizing mAbs, we selected the scFv-PSIF and IgG-NCS forms. Both forms were suitable models of ADCs because both drugs are used clinically as successful anticancer medicines.[10,43] First, the in vitro cell-killing activities of scFv-PSIFs and IgG-NCSes were estimated by a cytotoxicity assay with MS1 cells (Figure 5A-D). Both forms of cell-internalizing mAbs showed an approximately 10-fold higher cytotoxicity than the low-internalizing mAbs. These findings clearly suggest that internalization enhanced the delivery of conjugated drugs into the cells because our cell-internalizing mAbs and low-internalizing mAbs had similar affinities against antigens (Table 1).

As the therapy experiment in vivo, scFv-PSIFs and IgG-NCSes were intravenously injected into B16BL6 tumor–bearing mice once every 2 days for a total of 5 injections (Figure 5E-H). All cell-internalizing mAbs significantly suppressed tumor growth, whereas the antitumor effects of the low-internalizing antibodies were

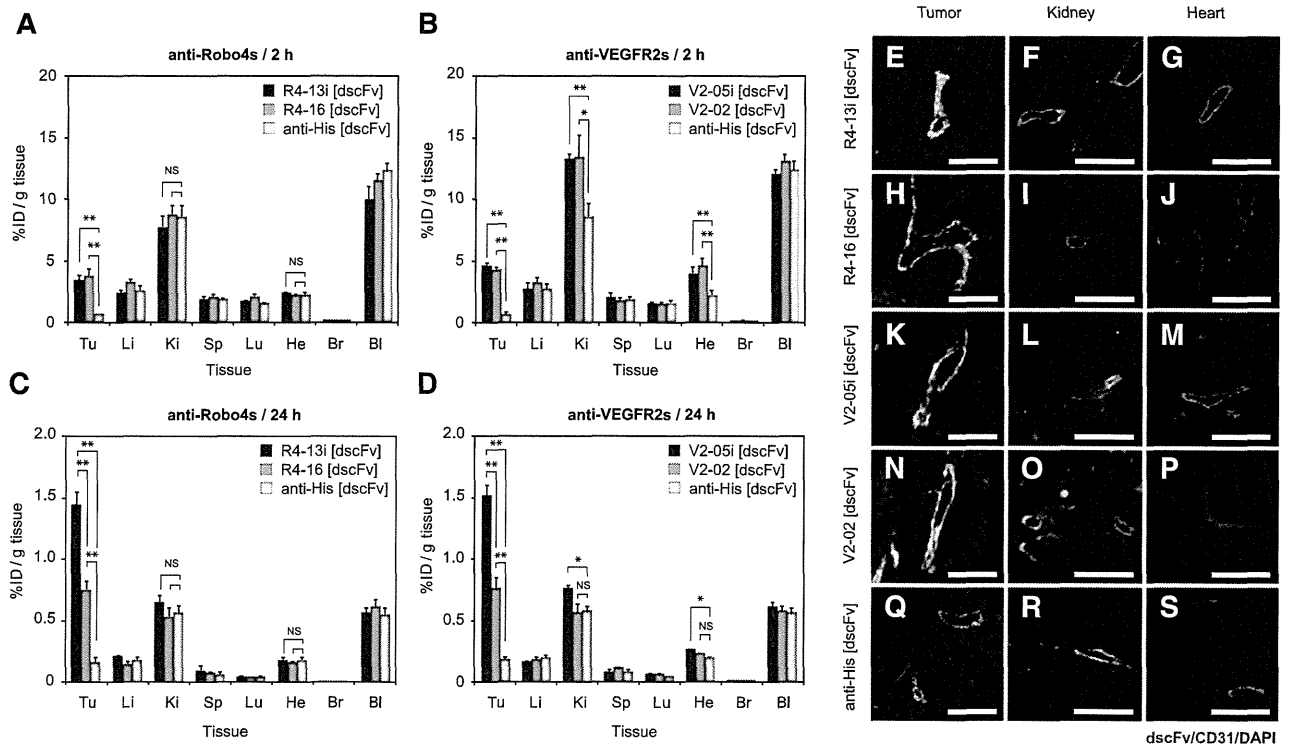

Figure 4. In vivo tumor-targeting activity of cell-internalizing mAbs. (A-D) Biodistribution of dscFvs in B16BL6 tumor–bearing mice. B16BL6 tumor–bearing mice were intravenously administered with anti-Robo4 dscFvs^{125I} (A,C) or anti-VEGFR2 dscFvs^{125I} (B,D). Each organ was extracted after 2 hours (A,B) or 24 hours (C,D), and the radioactivity was measured using a γ counter. %ID/g tissue was calculated using the following formula: %ID/g tissue = (count/g tissue)/(total injected count) × 100 (%). Tu, tumor; Li, liver; Ki, kidney; Sp, spleen; Lu, lung; He, heart; Br, brain; Bl, blood. (A,C) black; R4-13i[dscFv]^{125I}; gray, R4-16[dscFv]^{125I}; white, anti-His[dscFv]^{125I}. (B,D) black, V2-05i[dscFv]^{125I}; gray, V2-02[dscFv]^{125I}; white, anti-His[dscFv]^{125I}. Values are shown as means ± SEM. $^*P < .05$; $^{**}P < 0.01$; NS, not significant in Student's *t*-test ($n = 11$). (E-S) Co-immunostaining of dscFvs with CD31$^+$ blood endothelial cells on the tissue section. B16BL6 tumor–bearing mice were intravenously administered dscFvs^{Bio}. The tumor, kidney, and heart were extracted after 2 hours. Tissue sections of tumor, kidney, and heart were stained with streptavidin-PE conjugate. The blood vasculature was also stained with anti-CD31 antibody. Images were digitally merged. Red, dscFv^{Bio}; green, CD31; blue, DAPI (nucleus); yellow, colocalized region of red and green. Scale bar represents 100 μm. (E-G) R4-13i[dscFv]; (H-J) R4-16[dscFv]; (K-M) V2-05i[dscFv]; (N-P) V2-02[dscFv]; (Q-S) anti-His[dscFv]. (E,H,K,N,Q) Tumor section, (F,I,L,O,R) kidney section, and (G,J,M,P,S) heart section.

similar to those of the negative controls (anti-His[scFv]-PSIF and anti-FLAG[IgG]-NCS). The antitumor effects of R4-13i and V2-05i were similar in both ADC forms. These findings strongly suggest that the cell-internalizing activity of the mAbs was essential to maximize the delivery of the conjugated drug into the target cells, which significantly enhanced the antitumor effect of the ADCs.

Interestingly, the group of mice administered V2-05i[scFv]-PSIF had a significant loss of body weight, whereas the other groups did not (Figure 5I-L). As a preliminary result, 6 of 7 mice died in the V2-05i[scFv]-PSIF group with a similar protocol but with a fourfold higher dosage (60 pmol/mouse), perhaps because of the disruption of VEGFR2-positive cells in normal tissues by V2-05i[scFv]-PSIF, as shown in Figure 4. This side effect was not observed in the V2-05i [IgG]-NCS group. Therefore, we also hypothesized that the toxicity of NCS in normal cells was weak because NCS inhibits DNA synthesis in growing cells, such as tumor cells.[44] At a higher dosage, however, V2-05i[IgG]-NCS carries the risk of side effects. With regard to this point, none of the anti-Robo4 ADCs induced a loss of body weight; therefore, we concluded that Robo4 is a potential target for tumor vascular targeting with ADC.

Discussion

This study led to three novel findings. First, we demonstrated a rapid screening system for cell-internalizing mAbs in combination with the phage antibody library, which accelerated the identification of desired cell-internalizing mAbs. Second, comparative in vivo studies using cell-internalizing mAbs and low-internalizing mAbs with the same affinity values revealed that mAb internalization contributed to tumor targeting and enhanced the antitumor effects of the ADCs. Third, the first in vivo therapeutic application with anti-Robo4 mAb revealed that Robo4 is a therapeutic target on the tumor endothelial cells. The first and second findings will greatly contribute to the development of antibody therapies based on cell-internalizing antibodies such as ADCs, targeted liposomal drugs, or imaging. The third finding provides a new focus regarding the role of Robo4 biology in the body, such as the decreased side effects associated with depleting Robo4-positive endothelial cells in vivo.

This method allowed us to successfully isolate anti-Robo4 and anti-VEGFR2 cell-internalizing mAbs in combination with a phage antibody library and a PSIF-based screening system. This method provided one-step screening of cell-internalization of hundreds of "monoclonal" candidates. This is the main advantage of the present system over the old screening system, which required handling a "polyclonal" pool of mAbs.[6,7] The innovative feature of our method is the use of PSIF as a fusion partner for antibodies in scFv format, thus facilitating the identification of antibody fragments capable of efficient internalization. The scFv fusion is much easier than the chemical conjugation of the antibody to a cytotoxic drug. In principle, this method can be applied to other phage libraries, such as nonimmune phage antibody libraries[35,45] or synthetic

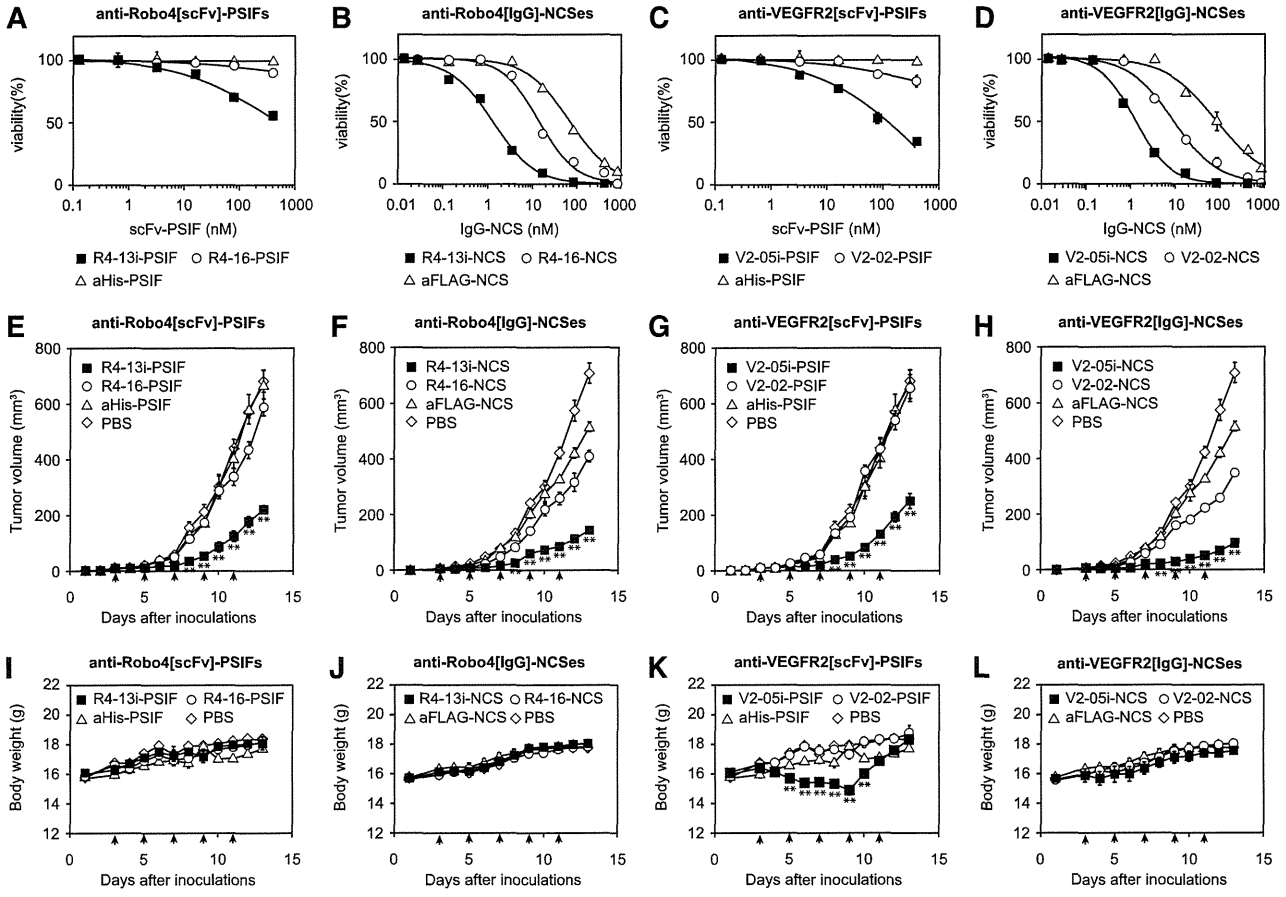

Figure 5. Enhanced anti-tumor effect of cell-internalizing mAbs. (A-D) Cytotoxicity of scFv-PSIF and IgG-NCS against MS1 cells. MS1 cells were incubated with serially diluted mAb-drug conjugates for 24 hours. Cell viability was then measured using a WST-8 assay. Closed square, internalizing mAbs; open circle, low-internalizing mAbs; open triangle, negative controls. (A) anti-Robo4[scFv]-PSIFs, (B) anti-Robo4[IgG]-NCSes, (C) anti-VEGFR2[scFv]-PSIFs, (D) anti-VEGFR2[IgG]-NCSes. Anti-His[scFv]-PSIF and anti-FLAG[IgG]-NCS were used as negative controls. Values are shown as means ± SD. (E-H) Antitumor effects of scFv-PSIFs or IgG-NCSes. B16BL6 cells were inoculated intracutaneously into C57BL6 mice on day 0. On days 3, 5, 7, 9, and 11, mAb-drug conjugates were intravenously administered *(arrow heads)*. Tumor volume was calculated using the following formula: tumor volume (mm^3) = {major axis of tumor (mm)} × {minor axis of tumor (mm)}^{2} × 0.4. Closed square, internalizing mAbs; open circle, low-internalizing mAbs; open triangle, negative controls (anti-His[scFv]-PSIF or anti-FLAG[IgG]-NCS); open diamond, PBS. (E) Anti-Robo4[scFv]-PSIFs, (F) anti-Robo4[IgG]-NCSes, (G) anti-VEGFR2[scFv]-PSIFs, (H) anti-VEGFR2[IgG]-NCSes. Values are shown as means ± SEM. $^{**}P < 0.01$; internalizing mAbs versus low-internalizing mAbs by Bonferroni post hoc analysis with two-way ANOVA (n = 6). (I-L) Change in body weight during therapy experiment. Closed square, internalizing mAbs; open circle, low-internalizing mAbs; open triangle, negative controls (anti-His[scFv]-PSIF or anti-FLAG[IgG]-NCS); open diamond, PBS. (I) anti-Robo4[scFv]-PSIFs, (J) anti-Robo4[IgG]-NCSes, (K) anti-VEGFR2[scFv]-PSIFs, (L) anti-VEGFR2[IgG]-NCSes. Values are shown as means ± SEM. $^{**}P < 0.01$; internalizing mAbs versus PBS by Bonferroni post hoc analysis with two-way ANOVA (n = 6).

human phage antibody libraries,[46,47] which have already been developed. This system can expand the versatility of phage display systems, which will thus contribute to the development of other cell-internalizing antibodies against various types of antigens for effective cancer therapy.

A comparison of cell-internalizing mAbs with low-internalizing mAbs revealed the strength of the cell-internalizing mAbs in terms of the biodistribution and therapeutic effects. Until now, how internalization contributes to the biodistribution of mAbs has been unclear. In this report, we could use a comparative study to clarify this question because we produced both cell-internalizing mAbs and low-internalizing mAbs with similar binding affinities. As a result, more cell-internalizing mAbs than low-internalizing mAbs were significantly accumulated in the tumor. This is the first evidence to support that mAbs with high internalization activity have greater tumor-targeting potency. This information is also useful for other applications that benefit from cell-internalizing mAbs, such as liposomal drugs, bioactive proteins/peptides, and viral vectors.[48,49]

Until now, the usefulness of Robo4-targeted therapy has not been established. Therapy to target VEGF-VEGFR signaling is already common, but the risk of side effects must be addressed.[31-33] Although VEGFR expression is upregulated on tumor vessels, it is also observed on the endothelium in healthy tissues. Previous reports also mentioned the toxicity associated with the anti-VEGFR therapies in mouse models[50] and the clinical trial.[51] Therefore, alternative therapies that target tumor angiogenesis are desired. In the present study, we revealed the possibility that anti-Robo4 ADCs were safer than anti-VEGFR2 ADCs, although they had similar antitumor effects. The findings from immunofluorescence and biodistribution studies also support the notion that anti-Robo4 mAbs could accumulate in the tumor without distributing to normal tissues. This is the first finding of Robo4-targeted therapy and suggests that Robo4 is a potential alternative target for tumor vascular targeting. Of course, additional experiments are needed to establish anti-Robo4 as a novel tool in tumor vascular targeting. For example, the pathological observations of normal blood vessels, in-depth toxicological analysis,

or the efficacy against other clinical relevant tumor models, are important for the successful story. Such basic analyses regarding Robo4 might accelerate the development of novel medicines that target tumor angiogenesis, including anti-Robo4 ADCs.

Acknowledgments

This study was supported by Grant-in-Aid for Scientific research (B) and Grant-in-Aid for Scientific Research on Innovative Areas from the Ministry of Education, Culture, Sports, Science, and Technology of Japan and the Japan Society for the Promotion of Science; Strategic Japanese-Swiss Cooperative Program from Japan Science and Technology Agency (JST) and the Swiss Federal Institute of Technology Zurich.

Authorship

Contribution: Y.M. designed the study; M.Y. and Y. Tsumori performed the experiments; Y.M. and M.Y. analyzed the data; Y.M. and M.Y. wrote the initial manuscript; S.T. and Y. Tsutsumi contributed to the phage display; Y.Y. and N.O. contributed to animal experiments; Y.O., W.C.A., and T.D. contributed to Robo4 related analysis; Y.M. and S.N. were responsible for the overall project. All authors edited the manuscript.

Conflict-of-interest disclosure: The authors declare no competing financial interests.

Correspondence: Yohei Mukai and Shinsaku Nakagawa, Laboratory of Biotechnology and Therapeutics, Graduate School of Pharmaceutical Sciences, Osaka University, 1–6 Yamadaoka, Suita, Osaka 565–0871, Japan; e-mail: y-mukai@nibio.go.jp and nakagawa@phs.osaka-u.ac.jp.

References

1. Alley SC, Okeley NM, Senter PD. Antibody-drug conjugates: targeted drug delivery for cancer. *Curr Opin Chem Biol.* 2010;14(4):529-537.
2. Isakoff SJ, Baselga J. Trastuzumab-DM1: building a chemotherapy-free road in the treatment of human epidermal growth factor receptor 2-positive breast cancer. *J Clin Oncol.* 2011;29(4): 351-354.
3. Ansell SM. Brentuximab vedotin: delivering an antimitotic drug to activated lymphoma cells. *Expert Opin Investig Drugs.* 2011;20(1):99-105.
4. Reichert JM. Antibody-based therapeutics to watch in 2011. *MAbs.* 2011;3(1):76-99.
5. Gerber HP, Senter PD, Grewal IS. Antibody drug-conjugates targeting the tumor vasculature: Current and future developments. *MAbs.* 2009; 1(3):247-253.
6. Poul MA, Becerril B, Nielsen UB, et al. Selection of tumor-specific internalizing human antibodies from phage libraries. *J Mol Biol.* 2000;301(5): 1149-1161.
7. An F, Drummond DC, Wilson S, et al. Targeted drug delivery to mesothelioma cells using functionally selected internalizing human single-chain antibodies. *Mol Cancer Ther.* 2008;7(3): 569-578.
8. Mukai Y, Sugita T, Yamato T, et al. Creation of novel Protein Transduction Domain (PTD) mutants by a phage display-based high-throughput screening system. *Biol Pharm Bull.* 2006;29(8):1570-1574.
9. Chaudhary VK, FitzGerald DJ, Adhya S, et al. Activity of a recombinant fusion protein between transforming growth factor type alpha and Pseudomonas toxin. *Proc Natl Acad Sci USA.* 1987;84(13):4538-4542.
10. Kreitman RJ, Wilson WH, Bergeron K, et al. Efficacy of the anti-CD22 recombinant immunotoxin BL22 in chemotherapy-resistant hairy-cell leukemia. *N Engl J Med.* 2001;345(4): 241-247.
11. Pastan I, FitzGerald D. Pseudomonas exotoxin: chimeric toxins. *J Biol Chem.* 1989;264(26): 15157-15160.
12. Legg JA, Herbert JMJ, Clissold P, et al. Slits and Roundabouts in cancer, tumour angiogenesis and endothelial cell migration. *Angiogenesis.* 2008; 11(1):13-21.
13. Huminiecki L, Bicknell R. In silico cloning of novel endothelial-specific genes. *Genome Res.* 2000; 10(11):1796-1806.
14. Huminiecki L, Gorn M, Suchting S, et al. Magic roundabout is a new member of the roundabout receptor family that is endothelial specific and expressed at sites of active angiogenesis. *Genomics.* 2002;79(4):547-552.
15. Smith-Berdan S, Nguyen A, Hassanein D, et al. Robo4 cooperates with CXCR4 to specify hematopoietic stem cell localization to bone marrow niches. *Cell Stem Cell.* 2011;8(1):72-83.
16. Park KW, Morrison CM, Sorensen LK, et al. Robo4 is a vascular-specific receptor that inhibits endothelial migration. *Dev Biol.* 2003;261(1): 251-267.
17. Seth P, Lin Y, Hanai J, et al. Magic roundabout, a tumor endothelial marker: expression and signaling. *Biochem Biophys Res Commun.* 2005; 332(2):533-541.
18. Okada Y, Yano K, Jin E, et al. A three-kilobase fragment of the human Robo4 promoter directs cell type-specific expression in endothelium. *Circ Res.* 2007;100(12):1712-1722.
19. Okada Y, Jin E, Nikolova-Krstevski V, et al. A GABP-binding element in the Robo4 promoter is necessary for endothelial expression in vivo. *Blood.* 2008;112(6):2336-2339.
20. Jones CA, London NR, Chen H, et al. Robo4 stabilizes the vascular network by inhibiting pathologic angiogenesis and endothelial hyperpermeability. *Nat Med.* 2008;14(4):448-453.
21. Jones CA, Nishiya N, London NR, et al. Slit2-Robo4 signalling promotes vascular stability by blocking Arf6 activity. *Nat Cell Biol.* 2009; 11(11):1325-1331.
22. Marlow R, Binnewies M, Sorensen LK, et al. Vascular Robo4 restricts proangiogenic VEGF signaling in breast. *Proc Natl Acad Sci USA.* 2010;107(23):10520-10525.
23. Koch AW, Mathivet T, Larrivée B, et al. Robo4 maintains vessel integrity and inhibits angiogenesis by interacting with UNC5B. *Dev Cell.* 2011;20(1):33-46.
24. Kerbel RS. Tumor angiogenesis. *N Engl J Med.* 2008;358(19):2039-2049.
25. Paleolog EM. Angiogenesis in rheumatoid arthritis. *Arthritis Res.* 2002;4(Suppl 3):S81-S90.
26. Tonnesen MG, Feng X, Clark RA. Angiogenesis in wound healing. *J Investig Dermatol Symp Proc.* 2000;5(1):40-46.
27. Olsson AK, Dimberg A, Kreuger J, et al. VEGF receptor signalling - in control of vascular function. *Nat Rev Mol Cell Biol.* 2006;7(5):359-371.
28. Crawford Y, Ferrara N. VEGF inhibition: insights from preclinical and clinical studies. *Cell Tissue Res.* 2009;335(1):261-269.
29. Wicki A, Rochlitz C, Orleth A, et al. Targeting tumor-associated endothelial cells: anti-VEGFR2 immunoliposomes mediate tumor vessel disruption and inhibit tumor growth. *Clin Cancer Res.* 2012;18(2):454-464.
30. Witmer AN, Dai J, Weich HA, et al. Expression of vascular endothelial growth factor receptors 1, 2, and 3 in quiescent endothelia. *J Histochem Cytochem.* 2002;50(6):767-777.
31. Kamba T, McDonald DM. Mechanisms of adverse effects of anti-VEGF therapy for cancer. *Br J Cancer.* 2007;96(12):1788-1795.
32. Eremina V, Jefferson JA, Kowalewska J, et al. VEGF inhibition and renal thrombotic microangiopathy. *N Engl J Med.* 2008;358(11):1129-1136.
33. Choueiri TK, Mayer EL, Je Y, et al. Congestive heart failure risk in patients with breast cancer treated with bevacizumab. *J Clin Oncol.* 2011; 29(6):632-638.
34. Yoshikawa M, Mukai Y, Okada Y, et al. Ligand-independent assembly of purified soluble magic roundabout (Robo4), a tumor-specific endothelial marker. *Protein Expr Purif.* 2008;61(1):78-82.
35. Imai S, Mukai Y, Nagano K, et al. Quality enhancement of the non-immune phage scFv library to isolate effective antibodies. *Biol Pharm Bull.* 2006;29(7):1325-1330.
36. Yoshikawa M, Mukai Y, Tsunoda S, et al. Modifying the antigen-immunization schedule improves the variety of monoclonal antibodies obtained from immune-phage antibody libraries against HIV-1 Nef and Vif. *J Biosci Bioeng.* 2011; 111(5):597-599.
37. Yamamoto Y, Tsutsumi Y, Yoshioka Y, et al. Site-specific PEGylation of a lysine-deficient TNF-alpha with full bioactivity. *Nat Biotechnol.* 2003;21(5):546-552.
38. Hunter WM, Greenwood FC. Preparation of iodine-131 labelled human growth hormone of high specific activity. *Nature.* 1962;194:495-496.
39. Mellman I. Endocytosis and molecular sorting. *Annu Rev Cell Dev Biol.* 1996;12:575-625.
40. Holliger P, Hudson PJ. Engineered antibody fragments and the rise of single domains. *Nat Biotechnol.* 2005;23(9):1126-1136.
41. Pavlinkova G, Beresford GW, Booth BJ, et al. Pharmacokinetics and biodistribution of engineered single-chain antibody constructs of MAb CC49 in colon carcinoma xenografts. *J Nucl Med.* 1999;40(9):1536-1546.
42. Schneider DW, Heitner T, Alicke B, et al. In vivo biodistribution, PET imaging, and tumor accumulation of 86Y- and 111In-antimindin/RG-1,

engineered antibody fragments in LNCaP tumor-bearing nude mice. *J Nucl Med.* 2009; 50(3):435-443.

43. Maeda H. SMANCS and polymer-conjugated macromolecular drugs: advantages in cancer chemotherapy. *Adv Drug Deliv Rev.* 2001;46(1-3): 169-185.
44. Kappen LS, Goldberg IH. Activation and inactivation of neocarzinostatin-induced cleavage of DNA. *Nucleic Acids Res.* 1978; 5(8):2959-2967.
45. Okamoto T, Mukai Y, Yoshioka Y, et al. Optimal construction of non-immune scFv phage display libraries from mouse bone marrow and spleen established to select specific scFvs efficiently binding to antigen. *Biochem Biophys Res Commun.* 2004;323(2): 583-591.
46. Silacci M, Brack S, Schirru G, et al. Design, construction, and characterization of a large synthetic human antibody phage display library. *Proteomics.* 2005;5(9): 2340-2350.
47. Villa A, Lovato V, Bujak E, et al. A novel synthetic naïve human antibody library allows the isolation of antibodies against a new epitope of oncofetal fibronectin. *MAbs.* 2011; 3(3):264-272.
48. Sapra P, Allen TM. Internalizing antibodies are necessary for improved therapeutic efficacy of antibody-targeted liposomal drugs. *Cancer Res.* 2002;62(24):7190-7194.
49. Pastan I, Hassan R, Fitzgerald DJ, et al. Immunotoxin therapy of cancer. *Nat Rev Cancer.* 2006;6(7):559-565.
50. Chinnasamy D, Yu Z, Theoret MR, et al. Gene therapy using genetically modified lymphocytes targeting VEGFR-2 inhibits the growth of vascularized syngenic tumors in mice. *J Clin Invest.* 2010;120(11):3953-3968.
51. Nagayama H, Matsumoto K, Isoo N, et al. Gastrointestinal bleeding during anti-angiogenic peptide vaccination in combination with gemcitabine for advanced pancreatic cancer. *Clin J Gastroenterol.* 2010;3(6):307-317.

Biochemical and Biophysical Research Communications 431 (2013) 336–341

Contents lists available at SciVerse ScienceDirect

Biochemical and Biophysical Research Communications

journal homepage: www.elsevier.com/locate/ybbrc

An induced pluripotent stem cell-mediated and integration-free factor VIII expression system

Yuwna Yakura [a,b,g], Chie Ishihara [b], Hajime Kurosaki [a], Yasuhiro Kazuki [a,c], Norio Komatsu [d], Yoshiaki Okada [e], Takefumi Doi [e], Hiroyuki Takeya [b,f], Mitsuo Oshimura [a,c,h,*]

[a] Department of Biomedical Science, Institute of Regenerative Medicine and Biofunction, Graduate School of Medical Science, Tottori University, Tottori, Japan
[b] Division of Pathological Biochemistry, Department of Life Sciences, Tottori University School of Medicine, Tottori, Japan
[c] Chromosome Engineering Research Center, Tottori University, Tottori, Japan
[d] Department of Hematology, Juntendo University School of Medicine, Japan
[e] Graduate School of Pharmaceutical Sciences, Osaka University, Osaka, Japan
[f] Department of Applied Life Science, Faculty of Biotechnology and Life Science, Sojo University, Kumamoto, Japan
[g] JSPS Research Fellowships for Young Scientists, Tokyo, Japan
[h] JST, CREST, Tokyo, Japan

ARTICLE INFO

Article history:
Received 10 December 2012
Available online 3 January 2013

Keywords:
Human artificial chromosome
Induced pluripotent stem cells
Sendai virus vector
Integration-free
Hemophilia A
Factor VIII

ABSTRACT

Human artificial chromosome (HAC) has several advantages as a gene therapy vector, including stable episomal maintenance and the ability to carry large gene inserts. Induced pluripotent stem (iPS) cells also have a great potential for gene therapy, which can be generated from an individual's own tissues and contribute to any tissues when reintroduced. A Sendai virus (SeV) vector with reprogramming factors is a powerful tool for generating iPS cells because of the high infection efficiency without the risk of integration into host chromosomes. In this study, we developed an iPS cell-mediated and integration-free coagulation factor VIII (FVIII) expression system using non-integrating SeV- and HAC-vectors. Multiple human FVIII genes, which were under the control of the megakaryocyte-specific platelet factor-4 (PF4) promoter for development of a treatment for hemophilia A, were inserted into a HAC vector (PF4-FVIII-HAC). The PF4-FVIII-HAC was introduced into SeV vector-mediated iPS cells derived from a mouse model of hemophilia A. After *in vitro* differentiation of iPS cells with the PF4-FVIII-HAC into megakaryocytes/platelets, the PF4-FVIII-HAC resulted in expression of FVIII. This study has developed the iPS cell-mediated PF4-driven FVIII expression system using two non-integrating vectors; therefore, this system may be a promising tool for safer gene- and cell-therapy of hemophilia A.

1. Introduction

Hemophilia A is an X chromosome-linked hemorrhagic disorder caused by defects in the coagulation factor VIII (FVIII) gene [1]. Current treatment consists of factor replacement with plasma-derived or recombinant FVIII products. However, these therapies are limited by the risk of infectious disease, the need for frequent injections, and the high cost of treatment [2]. Alternatively, gene therapy is an attractive approach for the treatment of hemophilia A, because a relatively modest increase in FVIII levels results in a sufficient therapeutic effect and it may provide sustained levels of FVIII. Hence, many groups have previously developed various strategies for gene therapy of hemophilia [3–5]. However, the ultimate cure for hemophilia by gene therapy has not been achieved because of several issues with conventional vector systems as follows; (1) the limited packaging capacity of vector particles, (2) the risk of oncogene activation caused by insertional mutagenesis, (3) over-expression or silencing, and (4) immune responses to the viral capsid [6].

Human artificial chromosome (HAC) vectors show considerable promise for gene therapy applications because they are stably maintained independent of host chromosomes as a mini-chromosome, thus diminishing or eliminating the risk of insertional mutagenesis [7]. In addition, HACs have the capacity to deliver an extremely large genomic region, such as 5 Mb [8], and allow physiological regulation of the introduced gene in a manner similar to that of the native chromosome [9–11]. Therefore, the use of HACs as a vector for gene therapy can solve the problems of conventional vectors, and are expected to be used for future gene- and cell-therapy.

Induced pluripotent stem (iPS) cells also have a great potential for gene therapy, which can be generated from an individual's own

* Corresponding author. Address: Department of Biomedical Science, Institute of Regenerative Medicine and Biofunction, Graduate School of Medical Science, 86 Nishi-cho, Yonago, Tottori 683-8503, Japan. Fax: +81 859 38 6210.
E-mail address: oshimura@grape.med.tottori-u.ac.jp (M. Oshimura).

0006-291X/$ - see front matter © 2013 Elsevier Inc. All rights reserved.
http://dx.doi.org/10.1016/j.bbrc.2012.12.096

tissues and contribute to the specialized function of any tissue when reintroduced. However, a problem with iPS cell induction is integration of transgenes into host chromosomes, which includes the risk of oncogene activation [12]. Sendai virus (SeV) exists as a form of negative-sense single-stranded RNA in the cytoplasm of infected cells. Therefore, a SeV vector with reprogramming factors has been a solution for induction of integration-free iPS cells [13].

In the present study, we used the megakaryocyte-specific platelet factor-4 (PF4) promoter [14], and established a HAC vector containing multiple FVIII expression cassettes under the control of the PF4 promoter. We transferred the HAC vector into hemophilia A model mouse iPS (FVIII KO-iPS) cells induced by the SeV vector with reprogramming factors, and examined whether the HAC vector is able to induce FVIII expression in megakaryocytes. Although we must perform *in vivo* experiments to demonstrate the safety and efficiency of this strategy, the present findings suggest that this approach may be a promising strategy for safe gene- and cell-therapy of hemophilia A.

2. Materials and methods

2.1. Vector construction

We previously developed a P1 bacteriophage artificial chromosome (pPAC)-FVIII vector with FVIII under the control of the cytomegalovirus immediate early enhancer-chicken β-actin hybrid (CAG) promoter [15]. In this study, the CAG promoter was excised by *XhoI* and replaced by the human megakaryocyte-specific PF4 promoter [14]. Multiple tandem copies of the FVIII expression cassette were constructed using compatible restriction sites. The FVIII expression cassette was excised by *AscI* and *AvrII*, and cloned into the pPAC-PF4-FVIII vector digested by *AscI* and *NheI*. Using this strategy, we obtained pPAC-PF4-FVIII with two and four copies of the FVIII expression cassette.

2.2. Cell culture

Hypoxanthine phosphoribosyl transferase (HPRT)-deficient Chinese hamster ovary (CHO) cells (JCR B0218) containing the HAC vector were cultured at 37 °C with 5% CO_2 in Ham's F-12 nutrient mixture (Invitrogen) plus 10% fetal bovine serum (FBS) with 8 μg/ml blasticidin S (BS; Funakoshi). Mouse iPS cells (see Section 2.8) were maintained on mitomycin C (Sigma)-treated mouse embryonic fibroblasts (MEFs) at 37 °C with 5% CO_2 in Dulbecco's modified Eagle's medium (Wako) containing 20% FBS, 1 mM sodium pyruvate (Invitrogen), 0.1 mM nonessential amino acids (Invitrogen), 2 mM L-glutamine (Invitrogen), 0.1 mM 2-mercaptoethanol (Sigma), and 1,000 U/ml leukemia inhibitory factor (Funakoshi).

2.3. Transient transfection

Human megakaryoblastic leukemia cell line UT-7/GM cells [16] were maintained in Iscove's modified Dulbecco's medium (Invitrogen) containing 10% FBS and 1 ng/ml granulocyte–macrophage colony-stimulating factor (GM-CSF; Sigma). Cells were washed twice in PBS and resuspended in K-PBS buffer (31 mM NaCl, 120.7 mM KCl, 8.1 mM Na_2HPO_4, 1.46 mM KH_2PO_4, and 10 mM $MgCl_2$) to a final concentration of 2×10^6 cells per 100 μl. These cells were mixed with each pPAC-PF4-FVIII vector, exposed to an exponential discharge of 150 V from a 25 μF capacitor using a Gene Pulser apparatus (Bio-Rad), and then transferred into culture medium. For induction of megakaryocytes/platelets differentiation, UT-7/GM cells were cultured for 72 h with 10 ng/ml thrombopoietin (TPO; a gift from Kirin Brewery) in place of GM-CSF.

2.4. Construction of PF4-FVIII-HAC

Modified pPAC-PF4-FVIII and Cre-recombinase expression vectors (pBS185; Invitrogen) were co-transfected into CHO cells containing the 21HAC2 vector [8] using Lipofectamine 2000 (Invitrogen) according to the manufacturer's instructions. After 24 h of culture in basic growth medium, cells were cultured in medium containing hypoxanthine–aminopterin–thymidine (HAT; Sigma). After 12 days of selection, HAT-resistant colonies were picked up and expanded for genomic PCR and fluorescence *in situ* hybridization (FISH) analyses.

2.5. Microcell-mediated chromosome transfer (MMCT)

MMCT was performed as described previously [17]. CHO cells containing PF4-FVIII-HAC were used as donor microcell hybrids. Briefly, mouse iPS cells were fused with microcells prepared from donor hybrid CHO cells, and then selected with BS (10 μg/ml). The transferred PF4-FVIII-HAC in each cell line was characterized by genomic PCR and FISH analyses.

2.6. Genomic PCR analyses

Genomic DNA was extracted from host cells containing PF4-FVIII-HAC using a Gentra Puregene Cell Kit (Qiagen), and PCR was performed using the following primers: FVIII-1 (sense, 5′-ggatcacctttcaacatcg-3′; and antisense, 5′-tcttgaactgagggacactg-3′), FVIII-2 (sense, 5′-atacaacgctttctccccaa-3′; and antisense, 5′-gttcagtgtgttagtgtggc-3′), PF4 (sense, 5′-catatagttgtcagggaaggg-3′; and antisense, 5′-ggctgtttcttcattgtttcc-3′), and HPRT (sense, 5′-tggaggccataaacaagaagac-3′; and antisense, 5′-ccccttgacccagaaattcca-3′).

2.7. FISH analyses

FISH analyses were performed using either fixed metaphase or interphase spreads of each cell hybrid using digoxigenin-labeled (Roche) human Cot-1 DNA (Invitrogen) and biotin-labeled pPAC-PF4-FVIII DNA probes as described previously [17]. Chromosomal DNA was counterstained with DAPI (Sigma). Images were captured using an NIS-Elements system (Nikon) and Axio Imager-Z2 (Carl Zeiss).

2.8. Induction of iPS cells

Induction of iPS cells from hemophilia A model mouse embryonic fibroblasts (FVIII KO-MEFs; Jackson Laboratory, strain name: 129S4-F8tm1Kaz/J, stock number: 004424) was performed using a SeV vector system (Dnavec) as described previously [13]. Briefly, four SeV vectors containing Oct3/4, Klf4, c-MYC and Sox2 were used to infect FVIII KO-MEFs. At 6 days after infection, FVIII KO-MEFs were re-plated at 5×10^4 cells per 10-cm dish on MEF feeder cells. The next day, the medium was replaced with mouse iPS cell medium. At 24 days after transfection, mouse iPS-like colonies were selected and transferred onto feeder cells in 6-well plates.

2.9. Immunofluorescence staining

Immunofluorescence staining was performed using a primary anti-SeV polyclonal antibody (Medical and Biological laboratories) after fixation with 4% paraformaldehyde in PBS. A secondary anti-rabbit IgG antibody conjugated with Alexa Fluor 594 (Molecular Probes) was used, followed by analysis with a fluorescence microscope (ECLIPSE Ti-U, Nikon).

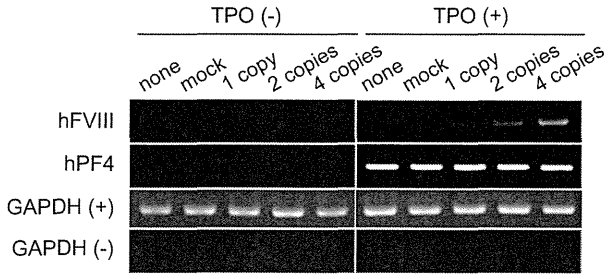

Fig. 1. UT-7/GM cells were transiently transfected with each of the pPAC-PF4-FVIII vectors (one, two and four copies) and cultured for 72 h with or without 10 ng/ml TPO. Total RNA was collected from these cells, and the levels of hPF4 and hFVIII mRNA were detected by RT-PCR. GAPDH was used as an internal control.

2.10. Differentiation of iPS cells

For differentiation into megakaryocytes/platelets, 1×10^4 iPS cells were seeded into each well of a 6-well plate containing confluent OP9 stromal cells (Riken BioResource Center) and cultured in α-MEM (Sigma) supplemented with 20% FBS and 1% L-glutamine [18]. After 5 days in culture, the cells were seeded onto a fresh OP9 layer in the same culture medium supplemented with 20 ng/ml human TPO. After 2 days of culture, the medium was changed every day. On day 12 of culture, FVIII expression was examined by RT-PCR.

2.11. RT-PCR

Total RNA was isolated from cells using Trizol (Invitrogen) and treated with a Turbo DNA-free kit (Ambion) to remove genomic DNA contamination. First-strand cDNA synthesis was performed using ReverTra Ace (Toyobo). After cDNA synthesis, cDNA was amplified by PCR using ExTaq (Takara). GAPDH and Nat1 were used as internal controls. PCR primers for amplification of each gene were as follows: Oct3/4 (SeV) (sense, 5′-cccgaaagagaaagcgaaccag-3′; and antisense, 5′-aatgtatcgaaggtgctcaa-3′), Sox2 (SeV) (sense, 5′-acaagagaaaaaacatgtatgg-3′; and antisense, 5′-atgcgctggttcacg cccgcgcccagg-3′), Klf4 (sense, 5′-acaagagaaaaaacatg tatgg-3′; and antisense, 5′-cgcgctggcagggccgctgctcgac-3′), c-MYC (sense, 5′-taac tgactagcaggcttgtcg-3′; and antisense, 5′-tccacatacagtcctggatgatgatg-3′), Oct4 (sense, 5′-tctttccaccaggcccccggctc-3′; and antisense, 5′-tgcgggcggacatggggagatcc-3′), Sox2 (endo) (sense, 5′-tagagctagactc cgggcgatga-3′; and antisense, 5′-ttgccttaaacaagaccacgaaa-3′), Nanog (sense, 5′-caggtgtttgagggtagctc-3′; and antisense, 5′-cggttcatcatgg-tacagtc-3′), Rex1 (sense, 5′-acgagtggcagtttcttcttggga-3′; and antisense, 5′-tatgactcacttccaggggcact-3′), hFVIII (sense, 5′-tctgccac actaacacactg-3′; and antisense, 5′-gggtcttgatgccgtgaata-3′), hPF4 (sense, 5′-agcatgagctccgcagccgggttct-3′; and antisense, 5′-cttccat tcttcagcgtggctatca-3′), mPF4 (sense, 5′-gtagaactttatctttgggt-3′; and antisense, 5′-aattttcctcccattcttca-3′), GAPDH (sense, 5′-ctcact-caagattgtcagca-3′; and antisense, 5′-gagttgggatagggcctc-3′), and Nat1 (sense, 5′-attcttcgttgtcaagccgccaaagtggag-3′; and antisense, 5′-agttgtttgctgcggagttgtcatctcgtc-3′). Amplified DNA fragments

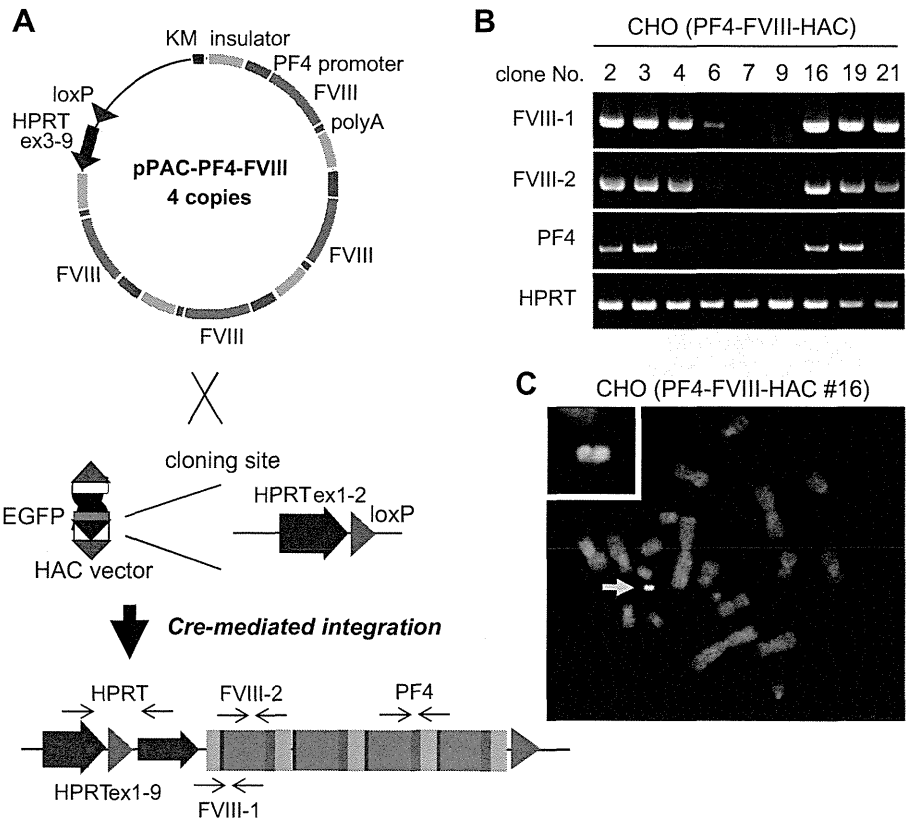

Fig. 2. (A) Schematic diagram of insertion of the FVIII expression cassette into the HAC vector. (B) Genomic PCR data of detecting PF4-FVIII-HAC in CHO cells. Each amplification site is mapped in (A, arrows). Representative data are shown. (C) FISH analysis of CHO cells. A digoxigenin-labeled human Cot 1 DNA probe (red) was used to detect the HAC vector. Biotin-labeled pPAC-PF4-FVIII (green) was used to detect the transgene on the HAC vector. Chromosomal DNA was counterstained with DAPI. The inset shows an enlarged image of the HAC vector (arrow). Representative data are shown.

were resolved by electrophoresis on a 2% agarose gel and visualized by ultraviolet fluorescence.

3. Results

3.1. Construction of the PF4-FVIII-HAC vector

To construct a HAC vector for gene expression of human FVIII (hFVIII) in megakaryocytes, the hFVIII gene was ligated to the human PF4 (hPF4) promoter. First, to demonstrate the ability of our construct to induce FVIII expression, human megakaryoblastic leukemia cell line UT-7/GM cells [16] was transiently transfected with each of the pPAC-PF4-FVIII vectors (one, two and four copies, see Section 2) (Fig. 1). Transfected cells were cultured with or without TPO, which has been shown to induce megakaryocytes/platelets differentiation of UT-7/GM cells [16], and differentiation into megakaryocytes/platelets was confirmed by detection of hPF4 mRNA expression (Fig. 1). As expected, hFVIII mRNA expression increased in a copy number-dependent manner.

The HAC vector contained a HPRT exon1-2-loxP cloning site into which circular DNA can be inserted using the Cre-loxP system. Eight micrograms of the pPAC-PF4-FVIII vector (four copies) was co-transfected with 1 μg of the Cre-recombinase expression plasmid into CHO cells containing an empty HAC vector (Fig. 2A). Twenty-eight HAT-resistant colonies were expanded and screened by genomic PCR analyses with primers for the FVIII transgene, PF4 promoter and reconstructed HPRT gene (Fig. 2A, arrow). Thirteen out of the twenty-eight HAT-resistant clones contained an intact PF4-FVIII-HAC (Fig. 2B), and then three clones were randomly selected for FISH analyses. FISH analyses with a biotin-labeled FVIII cDNA probe and digoxigenin-labeled human Cot1 DNA probe revealed that the presence of PF4-FVIII-HAC resulted in neither insertion nor translocation to the host chromosomes in two of the three clones (Fig. 2C).

3.2. Production of FVIII KO-iPS cells with the PF4-FVIII-HAC vector

FVIII KO-iPS cells were induced from FVIII KO-MEFs by infection with a SeV vector carrying four reprogramming factors, i.e., Oct3/4, Klf4, c-MYC and Sox2. Infected MEFs gave rise to iPS cell-like colonies that were isolated and expanded to cell lines. Two clones displaying a 40,*XY* normal metaphase were used for the following experiments (Fig. 3A).

PF4-FVIII-HAC vector was transferred into the two FVIII KO-iPS clones by MMCT. Because the HAC vector contained a green fluorescence protein (GFP) marker gene (Fig. 2A), after BS selection, GFP-positive clones were selected and examined in the following experiments (Fig. 3B). Thirteen of the resulting GFP-positive clones

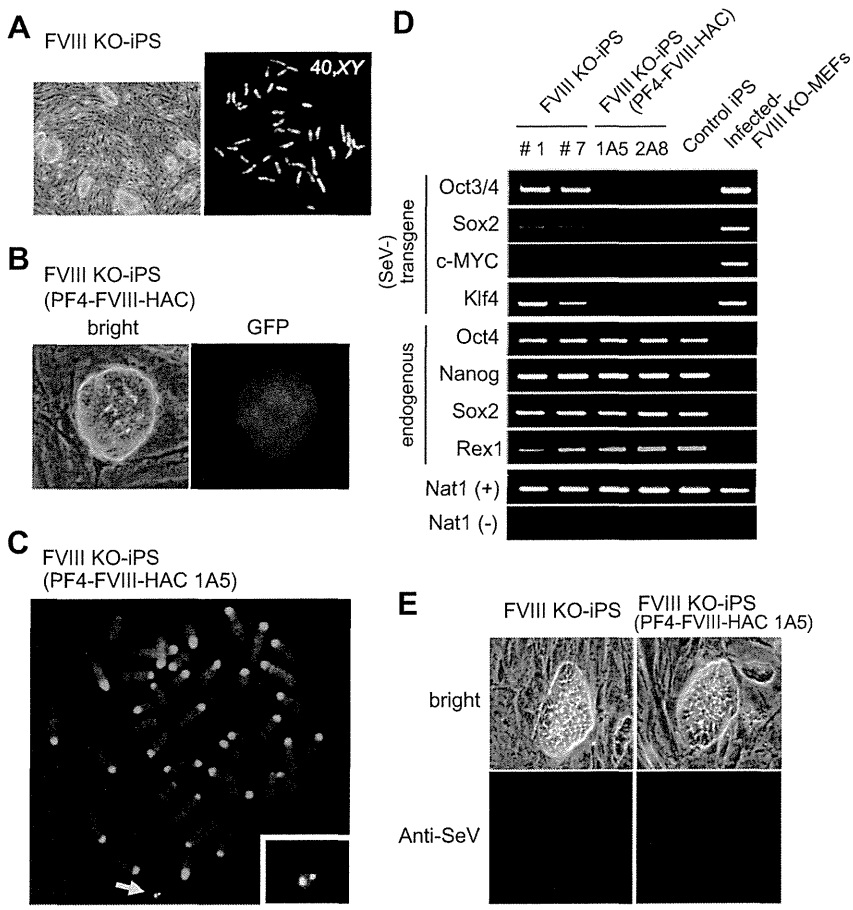

Fig. 3. Characterization of mouse iPS cells. (A) Morphology of FVIII KO-iPS clones (left panel). Q-banding metaphase are shown (right panel). (B) Morphology of FVIII KO-iPS (PF4-FVIII-HAC) cells. Bright field (left panel) and GFP fluorescence (right panel) microscopy images are shown. (C) FISH analysis of FVIII KO-iPS (PF4-FVIII-HAC) cells. A digoxigenin-labeled human Cot 1 DNA probe (red) was used to detect the HAC vector. Biotin-labeled pPAC-PF4-FVIII (green) was used to detect the transgene on the HAC vector. Chromosomal DNA was counterstained with DAPI. The inset shows an enlarged image of the HAC vector (arrow). Representative data are shown. (D) RT-PCR analyses of ES cell marker genes and four exogenous transcription factors. Nat1 was used as an internal control. Representative data are shown. (E) Immunostaining of parent FVIII KO-iPS cells and iPS cells containing PF4-FVIII-HAC. Bright field (top panel) and fluorescence (bottom panel) microscopy images are shown. Representative data are shown.

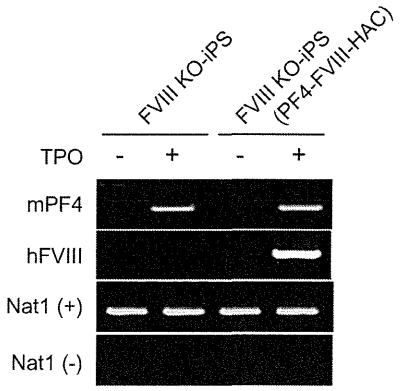

Fig. 4. *In vitro* differentiation of FVIII KO-iPS cells with or without PF4-FVIII-HAC. RT-PCR analyses of mPF4 and the hFVIII gene. Nat1 was used as an internal control.

were screened by genomic PCR analyses using primers to detect PF4-FVIII-HAC. Ten out of thirteen clones contained an intact PF4-FVIII-HAC (data not shown), and then FISH analyses showed that PF4-FVIII-HAC was present as an individual chromosome and normal karyotype in four clones (Fig. 3C). These four clones showed that the PF4-FVIII-HAC can be transferred to FVIII KO-iPS cells without affecting host chromosomes. Next, to test the stemness or undifferentiated state of these iPS cells, RT-PCR analyses using primers for embryonic stem (ES) cell-specific genes were performed. Endogenous Oct4, Nanog, Sox2 and Rex1 were expressed in two parent FVIII KO-iPS cell lines (#1 and #7) and all FVIII KO-iPS containing PF4-FVIII-HAC [FVIII KO-iPS (PF4-FVIII-HAC)] clones, comparable with that in control iPS cells (Fig. 3D). Exogenous SeV-transgenes, Oct3/4, Sox2, c-MYC and Klf4, were strongly or weakly expressed in two parent FVIII KO-iPS cell lines. However, expression of these genes was undetected in two FVIII KO-iPS (PF4-FVIII-HAC) clones (1A5 and 2A8) (Fig. 3D and E), suggesting that SeV-transgene expression was more or less decreased during cell division or after MMCT re-cloning. These results indicated that two clones (1A5 and 2A8) were SeV-free pluripotent stem cells and displayed a normal karyotype and independent PF4-FVIII-HAC vector.

3.3. Analyses of FVIII expression

We investigated whether *in vitro* megakaryocytes/platelets differentiation would result in FVIII expression. We cultured FVIII KO-iPS (PF4-FVIII-HAC) cells with TPO to induce differentiation, and then megakaryocytes/platelets differentiation was confirmed by detection of mPF4 mRNA expression (Fig. 4). FVIII expression was detected in megakaryocytes/platelets derived from FVIII KO-iPS (PF4-FVIII-HAC) cells, whereas undifferentiated cells showed no FVIII expression (Fig. 4). Taken together, these results show that PF4-FVIII-HAC vector accomplishes ectopic expression of FVIII in megakaryocytes/platelets derived from FVIII KO-iPS cells.

4. Discussion

Gene- and cell- therapy requires the development of an efficient and safe gene delivery system to be acceptable for clinical applications. Previously, both non-viral and viral vectors have been considered for the development of gene therapy of hemophilia in various animal models [3,19–21]. HAC vectors also support the correction of defective genes because expression from and transmission of these vectors are stable throughout many cell divisions [7,15,22]. In addition, because of their episomal nature, silencing of the introduced gene or oncogenesis resulting from integration into host chromosomes should be minimized. Another advantage of the HAC vector is transference into various cell types by MMCT methods without insertional mutagenesis. Nonetheless, the transfer rate of HAC via MMCT method is low, i.e., 10^5. Nevertheless, the MMCT frequency needs to improve. Moreover, in MMCT methods, it is possible to simultaneously transfer host chromosomes (e.g., CHO) along with the HAC. However, using FISH, karyotyping and RT-PCR, we have seldom observed co-transfer of host chromosomes during MMCT. Use of the HAC vector for FVIII expression is therefore expected to contribute to the development of new treatments for hemophilia A.

Integration of transgenes into host chromosomes is a major technical hurdle for clinical application. Although several methods for induction of iPS cells have been developed using adenoviruses [23] or plasmids [24], the risk of integration still remains while DNA vectors are used. In this study, we used a SeV vector, an RNA virus with no risk of altering host chromosomes, for iPS cell generation and successfully obtained exogenous transgene-free iPS cells. In addition, the HAC vector has a major advantage by being maintained independently of host chromosomes. Application of these methods to iPS cells combined with the HAC vector may be a powerful tool for safe gene- and cell- therapy.

In conclusion, we have developed HAC vectors containing multiple FVIII expression cassettes for gene therapy of hemophilia A, and transferred PF4-FVIII-HAC into SeV-free iPS cells, which is ectopically expressed in megakaryocytes/platelets. By combining integration-free iPS cells derived from patients [11,25,26], this HAC vector may be a promising strategy for novel and safe gene- and cell-therapy of hemophilia A. However, for such validation of the expression level or the therapeutic effect, *in vivo* experimental confirmation remains to be performed. Furthermore, several groups have reported that ectopic expression of the FVIII gene in megakaryocytes/platelets is therapeutic towards hemophilia A with inhibitory antibodies [27,28]; therefore, we need to verify the effect of inhibitory antibodies.

Funding

This work was supported in part by grants from the Ministry of Education, Culture, Sports, Science, and Technology of Japan (HT), the Japan Society for the Promotion of Science (YY) and the Japan Science and Technology Agency, CREST (MO).

Acknowledgments

We thank Sachiko Matsumoto for technical assistance.

References

[1] R.J. Kaufman, Advances toward gene therapy for hemophilia at the millennium, Hum. Gene Ther. 10 (1999) 2091–2107.
[2] K.A. High, Update on progress and hurdles in novel genetic therapies for hemophilia, Hematology Am. Soc. Hematol. Educ. Program (2007) 466–472.
[3] B.T. Kren, G.M. Unger, L. Sjeklocha, A.A. Trossen, V. Korman, B.M. Diethelm-Okita, M.T. Reding, C.J. Steer, Nanocapsule-delivered Sleeping Beauty mediates therapeutic Factor VIII expression in liver sinusoidal endothelial cells of hemophilia A mice, J. Clin. Invest. 119 (2009) 2086–2099.
[4] N.C. Hasbrouck, K.A. High, AAV-mediated gene transfer for the treatment of hemophilia B: problems and prospects, Gene Ther. 15 (2008) 870–875.
[5] D.W. Scott, J.N. Lozier, Gene therapy for haemophilia: prospects and challenges to prevent or reverse inhibitor formation, Br. J. Haematol. 156 (2012) 295–302.
[6] I. Petrus, M. Chuah, T. VandenDriessche, Gene therapy strategies for hemophilia: benefits versus risks, J. Gene Med. 12 (2010) 797–809.
[7] Y. Kazuki, M. Oshimura, Human artificial chromosomes for gene delivery and the development of animal models, Mol. Ther. 19 (2011) 1591–1601.
[8] Y. Kazuki, H. Hoshiya, M. Takiguchi, S. Abe, Y. Iida, M. Osaki, M. Katoh, M. Hiratsuka, Y. Shirayoshi, K. Hiramatsu, E. Ueno, N. Kajitani, T. Yoshino, K. Kazuki, C. Ishihara, S. Takehara, S. Tsuji, F. Ejima, A. Toyoda, Y. Sakaki, V. Larionov, N. Kouprina, M. Oshimura, Refined human artificial chromosome

vectors for gene therapy and animal transgenesis, Gene ther. 18 (2011) 384–393.
[9] Y. Kuroiwa, K. Tomizuka, T. Shinohara, Y. Kazuki, H. Yoshida, A. Ohguma, T. Yamamoto, S. Tanaka, M. Oshimura, I. Ishida, Manipulation of human minichromosomes to carry greater than megabase-sized chromosome inserts, Nat. Biotechnol. 18 (2000) 1086–1090.
[10] M. Katoh, F. Ayabe, S. Norikane, T. Okada, H. Masumoto, S. Horike, Y. Shirayoshi, M. Oshimura, Construction of a novel human artificial chromosome vector for gene delivery, Biochem. Biophys. Res. Commun. 321 (2004) 280–290.
[11] M. Oshimura, M. Katoh, Transfer of human artificial chromosome vectors into stem cells, Reprod. Biomed. Online 16 (2008) 57–69.
[12] K. Okita, T. Ichisaka, S. Yamanaka, Generation of germline-competent induced pluripotent stem cells, Nature 448 (2007) 313–317.
[13] N. Fusaki, H. Ban, A. Nishiyama, K. Saeki, M. Hasegawa, Efficient induction of transgene-free human pluripotent stem cells using a vector based on Sendai virus, an RNA virus that does not integrate into the host genome, Proc. Jpn. Acad. Ser. B Phys. Biol. Sci. 85 (2009) 348–362.
[14] Y. Okada, E. Matsuura, Z. Tozuka, R. Nagai, A. Watanabe, K. Matsumoto, K. Yasui, R.W. Jackman, T. Nakano, T. Doi, Upstream stimulatory factors stimulate transcription through E-box motifs in the PF4 gene in megakaryocytes, Blood 104 (2004) 2027–2034.
[15] H. Kurosaki, M. Hiratsuka, N. Imaoka, Y. Iida, N. Uno, Y. Kazuki, C. Ishihara, Y. Yakura, J. Mimuro, Y. Sakata, H. Takeya, M. Oshimura, Integration-free and stable expression of FVIII using a human artificial chromosome, J. Hum. Genet. 56 (2011) 727–733.
[16] N. Komatsu, K. Kirito, R. Shimizu, M. Kunitama, M. Yamada, M. Uchida, M. Takatoku, M. Eguchi, Y. Miura, *In vitro* development of erythroid and megakaryocytic cells from a UT-7 subline, UT-7/GM, Blood 89 (1997) 4021–4033.
[17] K. Tomizuka, H. Yoshida, H. Uejima, H. Kugoh, K. Sato, A. Ohguma, M. Hayasaka, K. Hanaoka, M. Oshimura, I. Ishida, Functional expression and germline transmission of a human chromosome fragment in chimeric mice, Nat. Genet. 16 (1997) 133–143.
[18] K. Eto, R. Murphy, S.W. Kerrigan, A. Bertoni, H. Stuhlmann, T. Nakano, A.D. Leavitt, S.J. Shattil, Megakaryocytes derived from embryonic stem cells implicate CalDAG-GEFI in integrin signaling, Proc. Natl. Acad. Sci. USA 99 (2002) 12819–12824.
[19] W.M. McCormack, M.P. Seiler, T.K. Bertin, K. Ubhayakar, D.J. Palmer, P. Ng, T.C. Nichols, B. Lee, Helper-dependent adenoviral gene therapy mediates long-term correction of the clotting defect in the canine hemophilia A model, J. Thromb. Haemost. 4 (2006) 1218–1225.
[20] D.A. Roth, N.E. Tawa, J.M. O'Brien, D.A. Treco, R.F. Selden, F.V.T.T.S. Group, nonviral transfer of the gene encoding coagulation factor VIII in patients with severe hemophilia A., N. Engl. J. Med. 344 (2001) 1735–1742.
[21] C.B. Doering, G. Denning, K. Dooriss, B. Gangadharan, J.M. Johnston, K.W. Kerstann, D.A. McCarty, H.T. Spencer, Directed engineering of a high-expression chimeric transgene as a strategy for gene therapy of hemophilia A, Mol. Ther. 17 (2009) 1145–1154.
[22] F.S. Tedesco, H. Hoshiya, G. D'Antona, M.F. Gerli, G. Messina, S. Antonini, R. Tonlorenzi, S. Benedetti, L. Berghella, Y. Torrente, Y. Kazuki, R. Bottinelli, M. Oshimura, G. Cossu, Stem cell-mediated transfer of a human artificial chromosome ameliorates muscular dystrophy, Sci Transl Med 3 (2011). 96ra78.
[23] M. Stadtfeld, M. Nagaya, J. Utikal, G. Weir, K. Hochedlinger, Induced pluripotent stem cells generated without viral integration, Science 322 (2008) 945–949.
[24] J. Yu, K. Hu, K. Smuga-Otto, S. Tian, R. Stewart, I.I. Slukvin, J.A. Thomson, Human induced pluripotent stem cells free of vector and transgene sequences, Science 324 (2009) 797–801.
[25] K. Takahashi, K. Tanabe, M. Ohnuki, M. Narita, T. Ichisaka, K. Tomoda, S. Yamanaka, Induction of pluripotent stem cells from adult human fibroblasts by defined factors, Cell 131 (2007) 861–872.
[26] D. Xu, Z. Alipio, L.M. Fink, D.M. Adcock, J. Yang, D.C. Ward, Y. Ma, Phenotypic correction of murine hemophilia A using an iPS cell-based therapy, Proc. Natl. Acad. Sci. USA 106 (2009) 808–813.
[27] T. Ohmori, J. Mimuro, K. Takano, S. Madoiwa, Y. Kashiwakura, A. Ishiwata, M. Niimura, K. Mitomo, T. Tabata, M. Hasegawa, K. Ozawa, Y. Sakata, Efficient expression of a transgene in platelets using simian immunodeficiency virus-based vector harboring glycoprotein Ibalpha promoter: *in vivo* model for platelet-targeting gene therapy, FASEB J. 20 (2006) 1522–1524.
[28] Q. Shi, D.A. Wilcox, S.A. Fahs, H. Weiler, C.W. Wells, B.C. Cooley, D. Desai, P.A. Morateck, J. Gorski, R.R. Montgomery, Factor VIII ectopically targeted to platelets is therapeutic in hemophilia A with high-titer inhibitory antibodies, J. Clin. Invest. 116 (2006) 1974–1982.